LUPINE PUBLISHERS

An archive of organic and inorganic chemical sciences

DOI: 10.32474/AOICS.2021.05.000216

ISSN: 2637-4609

Research Article

Synthesis, Crystal Structure and Spectroscopic Photoluminescence Proprieties of Organic-Inorganic Hybrid Compound Based on Iodidoplumbate (II) Motif

Oualid Mokhnache[1], Anna Gagor[2], Monika Trzebiatowska[2] and Habib Boughzala[1]*

[1]*Department of Chemistry, Faculty of Sciences of Tunis, Tunisia*

[2]*Institute of Low Temperature and Structure Research, Polish Academy of Science, Poland*

***Corresponding author:** Habib Boughzala, Department of Chemistry, Faculty of Sciences of Tunis, El Manar, Tunisia

Received: June 4, 2021 **Published:** August 02, 2021

Abstract

A new organic–inorganic hybrid material of formula 2[(CH_3) $C_6N_4H_{12}$] +[Pb2I6]2-. compound was obtained by slow evaporation at room temperature of a solution containing lead iodide and (NH_3) $C_6N_4H_{12}$ in a 1:2 molar ratio. Single crystal diffraction was carried out at 298 K and 100 K. The same P21/m monoclinic space group has been found for both temperatures. No structural difference has been noted apart from a typical increase of the cell parameters with temperature. The supramolecular structure cohesion is ensured by weak hydrogen bonding C–H···I interactions. The photoluminescence investigations reveal two distinct emission bands. The room-temperature infrared and Raman spectra are recorded. The theoretical infrared spectrum, crystal morphology and molecular orbital transition are calculated and discussed.

Keywords: Crystal structure; Organic-inorganic hybrid; Iodoplumbate (II); Hexamethylenetetramine; Hybrid compound; Vibrational studies; Photoluminescence; Optical properties.

Introduction

Recently, research of novel hybrid materials has become one of the most expanding fields in chemistry for several reasons [1]. In recent years, a significant number of organic-inorganic hybrid materials based on metal halide-units have been prepared and studied [2], particularly, the family of lead iodide-based crystals [3] and systems containing extended chains [4]. The lead iodide-based hybrid materials are extensively studied for their properties and self-organized structures [5]. Organic-inorganic hybrid offers the opportunity to combine the desirable properties of both organic and inorganic [6] moieties. The structural topology of the hybrid compounds can be tuned by adequate selection of anions, organic cation, the solvent type, and their proportion. The D-H…X (D=Donor, X = Cl, Br, I) hydrogen bonds and C-H…π or π…π interactions [4] are often directing the resulting structural arrangement and ensuring its cohesion [7]. The optical properties of the organic–inorganic compounds have been the focus of substantial current research studies owing to strong room temperature exciton emission [8]. In addition to tailoring the optical features by making substitutions on the metal or halogen sites, control over the specific structure of the metal halide sheets through the appropriate choice of the organic cations should provide a means for influencing the optical properties [9]. An important feature of organic–inorganic hybrids is their structural tunability. In fact, some structural differences are observed if the counter ions of the inorganic parts are monoprotonated or diprotonated amines [10]. The crystallographic orientation and the thickness of the inorganic sheets may vary according to the choice of the appropriate organic cations. In other words, inorganic units can be self-organized into low dimensional crystals, where they form zero-(0-D), one-(1-D), two-(2-D), or three-dimensional (3-D) networks adjusting to the organic cations [11]. The effective dimensionality of the extended inorganic anion has a significant impact on the physical properties of the hybrid materials [12].

Experimental

Synthesis and crystallization

Single crystals were prepared by slow evaporation at room temperature by mixing 1 mol of amino hexamethylenetetramine with 2 mol of lead iodide PbI2 dissolved in 5 ml of DMSO leading to an alkylation reaction. The obtained solution was evaporated slowly. Within few weeks, pyramidal yellow crystals were grown.

The crystals were extracted by filtration and dried for the single crystal X-ray diffraction study.

X-ray structure determination

A single crystal has been selected for X-ray diffraction analysis. Data collection was performed on an Oxford Diffraction Xcalibur four-circle diffractometer with CCD Atlas detector, operating at 298 K and 100 K with (Mo Kα radiation, λ= 0.71069 Å) [13]. The structures have been solved by direct methods using SHELXS-2014 software [14] and refined by least-square full-matrix based on F2 using SHELXL-2014 software [15] and SHELXLe [16]. A summary of the crystallographic data and structural determination for 2[$(CH_3)C_6N_4H_{12}$] +[Pb2I6]2-. is provided in (Table 1). The final reduced atomic coordinates and the equivalent Deby-Waller factors at 298 K and 100 K are listed in (Table 2). The thermal displacements of non-hydrogen atoms were refined in anisotropic mode (Table 3). The hydrogen atoms were localized using geometrical constraint conditions by adequate HFIX SHELXL options and parameters were refined in a common isotropic thermal model.

Table 1: Crystal data and summary of data collection and structure refinement at 298K and 100K.

Crystal data	T=298 K	T=100 K
Formula	$C_7H_{15}I_3N_4Pb$	
Formula weight	743.12	
Crystal system	Monoclinic	
space group	$P2_1/m$	
Temperature (K)	298	100
a(Å)	9.4375 (5)	9.3153 (4)
b(Å)	7.6678 (3)	7.5723 (3)
c(Å)	11.4143 (8)	11.3392 (6)
B (°)	110.060 (7)	109.810 (5)
Unit-cell volume (Å^3)	775.88 (7)	752.51(7)
Z	2	
Calculated density (g.cm^{-3})	3.181	3.28
Absorption coefficient (mm^{-1})	16.822	17.344
Data collection		
Temperature	298 K	100 K
Radiation, wavelength (Å)	MoKα, 0.71073	
F (000)	652	
θ_{max} (°)	29.335	29.4
h, k, l ranges	-8→13, -10→9, -14→11	-12→8, -9→9, -11→14
measured reflections	4189	4100
independent reflections	1959	1893
reflections with I > 2σ(I)	1479	1691
Refinement		
R [$F^2 > 2\sigma(F^2)$], wR(F^2), S	0.042, 0.130, 1.13	0.028, 0.0916, 1.19
Refinement method	Full-matrix least-squares on F^2	
No. of reflections	1959	1893
No. of parameters	83	83
H-atom treatment	H-atom parameters constrained	
$\Delta_{\rho max}$, $\Delta_{\rho min}$ (e Å^{-3})	2.30, -1.43	1.986, –1.621

Table 2: Fractional atomic coordinates and isotropic or equivalent isotropic displacement parameters (Å2)

	298 K				100 K			
Atom	**x**	**y**	**z**	**Uiso*/Ueq**	**x**	**y**	**z**	**Uiso*/Ueq**
Pb	2-Jan	2-Jan	2-Jan	0.036 (3)	2-Jan	2-Jan	2-Jan	0.011 (16)
I1	0.366 (10)	4-Jan	0.262 (9)	0.034 (3)	0.367 (7)	4-Jan	0.261 (6)	0.010 (18)
I2	0.660 (12)	4-Mar	0.349 (11)	0.042 (3)	0.661 (7)	4-Mar	0.347 (6)	0.013 (18)
I3	0.790 (11)	4-Jan	0.598 (10)	0.039 (3)	0.794 (7)	4-Jan	0.595 (6)	0.012 (18)
N1	0.640 (13)	4-Jan	0.059 (14)	0.044 (3)	0.637 (9)	4-Jan	0.059 (8)	0.012 (17)
N2	0.890 (13)	4-Jan	0.215 (12)	0.038 (3)	0.891 (9)	4-Jan	0.214 (8)	0.013 (17)
N3	0.842 (10)	0.407 (14)	0.023 (10)	0.051 (3)	0.841 (6)	0.411 (8)	0.018 (6)	0.014 (13)
C1	0.677 (12)	0.405 (17)	0.002 (13)	0.054 (3)	0.677 (8)	0.407 (9)	0.001 (7)	0.015 (15)
H1A	0.65	0.508	0.039	0.065*	0.651	0.511	0.038	0.019*
H1B	0.62	0.405	-0.081	0.065*	0.618	0.409	-0.087	0.019*
C2	0.923 (12)	0.410 (15)	0.152 (13)	0.050 (3)	0.927 (8)	0.412 (9)	0.150 (7)	0.014 (15)
H2A	0.896	0.513	0.189	0.060*	0.903	0.516	0.188	0.017*
H2B	1.031	0.415	0.166	0.060*	1.034	0.415	0.162	0.017*
C3	0.721 (18)	4-Jan	0.188 (16)	0.044 (4)	0.721 (11)	4-Jan	0.190 (10)	0.016 (2)
H3A	0.694	0.147	0.226	0.053*	0.695	0.147	0.228	0.019*
H3B	0.694	0.352	0.226	0.053*	0.695	0.352	0.228	0.019*
C4	0.880 (2)	4-Jan	-0.033 (16)	0.057 (5)	0.881 (11)	4-Jan	-0.034 (9)	0.017 (2)
H4A	0.823	4-Jan	-0.122	0.068*	0.829	4-Jan	-0.124	0.021*
H4B	0.986	4-Jan	-0.022	0.068*	0.988	4-Jan	-0.019	0.021*
C5	0.974 (2)	4-Jan	0.349 (18)	0.075 (6)	0.982 (12)	4-Jan	0.349 (10)	0.026 (3)
H5A	0.948	0.147	0.386	0.112*	0.958	0.147	0.387	0.039*
H5B	1.08	4-Jan	0.364	0.112*	1.087	4-Jan	0.36	0.039*
H5C	0.948	0.352	0.386	0.112*	0.958	0.352	0.387	0.039*

Table 3: Anisotropic atomic displacement parameters (Å2).

	298 K					100 K					
Atom	**U11**	**U22**	**U33**	**U12**	**U13**	**U23**	**U11**	**U22**	**U33**	**U12**	**U13**	**U23**
Pb	0.040 (4)	0.027 (4)	0.037 (4)	0.0002 (2)	0.0096 (3)	-0.0016 (2)	0.012 (2)	0.008 (2)	0.011 (2)	0.00010 (14)	0.002 (15)	-0.00043 (1)
I1	0.032(5)	0.038(6)	0.028(6)	0	0.0070(4)	0	0.009(3)	0.012(3)	0.009(3)	0	0.002(2)	0
I2	0.047(6)	0.043(6)	0.039(7)	0	0.0172(5)	0	0.014(3)	0.013(3)	0.012(4)	0	0.005(3)	0
I3	0.033(5)	0.042(6)	0.039(7)	0	0.0078(4)	0	0.010(3)	0.013(3)	0.011(3)	0	0.002(2)	0
N1	0.023(6)	0.057(9)	0.048(9)	0	0.007(6)	0	0.008(4)	0.013(4)	0.015(5)	0	0.003(3)	0
N2	0.029(6)	0.057(9)	0.025(7)	0	0.005(5)	0	0.014(4)	0.020(4)	0.005(4)	0	0.002(3)	0
N3	0.038(5)	0.062(7)	0.052(7)	0.000(5)	0.014(5)	0.015(6)	0.013(3)	0.019(3)	0.010(3)	0.000(3)	0.003(2)	0.005(3)
C1	0.029(6)	0.064(9)	0.059(9)	0.011(6)	0.002(6)	0.009(7)	0.014(3)	0.016(4)	0.017(4)	0.000(3)	0.006(3)	0.001(3)
C2	0.035(6)	0.038(7)	0.072(1)	0.002(5)	0.011(6)	-0.013(7)	0.015(3)	0.011(3)	0.015(4)	0.002(3)	0.003(3)	0.004(3)
C3	0.047(9)	0.059(10)	0.037(1)	0	0.029(8)	0	0.008(4)	0.025(6)	0.020(6)	0	0.012(4)	0
C4	0.049(10)	0.097(16)	0.023(9)	0	0.011(8)	0	0.010(5)	0.034(6)	0.007(5)	0	0.000(4)	0
C5	0.066(13)	0.120(2)	0.036(1)	0	0.018(10)	0	0.017(5)	0.051(8)	0.008(5)	0	0.002(4)	0

IR and Raman spectroscopy

The infrared spectrum was measured using KBr pellet with 2% weight compound by a Nicolet iS50 FT-IR spectrometer between 400 and 3500 cm^{-1}. The Raman spectrum was measured using a Renishaw InVia Raman spectrometer equipped with confocal DM 2500 Leica optical microscope, a thermoelectrically cooled CCD as a detector and an argon laser operating at 514 nm. Both IR and Raman spectra were recorded with a spectral resolution of 2 cm^{-1}.

Photoluminescence

The photoluminescence (PL) spectrum of the title compound spin coating film was recorded at room [17] temperature with Perkin- Elmer LS 55 fluorescence spectrometer.

Results and discussion

Global description

In both temperatures (298 K and 100 K) the compound crystallizes in the P21/m monoclinic space group. No structural modification has been observed. The structural unit consists of an octahedral PbI6 unit and a couple of aminohexamethylenetetramine cation. Exception for C1, C2, N3 and some hydrogen atomic positions, the main part of the asymmetric unit atoms are in special positions. [18-21] The structural unit of the crystal structure obtained at 298 K is shown in (Figure 1). Selected bond length and angles at temperatures, 298 K and 100 K are gathered in (Table 4). The electrical neu trality is ensured by two protonated organic molecules leading to the chemical formula $2[(CH_3)\ C_6N_4H_{12}]+[Pb2I6]2^-$ The crystal structure is composed of infinite octahedral face sharing [PbI6] anions and isolated monoprotonated 1-amino-1,3,5,7-tetraazaadamantan-1-ium. The [PbI6] ∞ chain is formed by face-sharing PbI6 octahedra represented in (Figure 4). The main part of the inorganic moiety is built of the lead Pb2+ cation adopting a distorted octahedral coordination. Three adjacent corners connect the octahedron to its neighbor, leading to zigzag chains running along the $\vec{b}$ axis. I1, I2 and I3 and their symmetric are bonded to Pb atom as shown in Figure 1. The resulting one-dimensional anionic network leaves empty spaces lodging the organic cations. At both temperatures (289 K & 100K), the inorganic anion can be considered as a set of face-shared octahedra establishing weak hydrogen interactions with the organic cations via C—H···I as represented in (Figure 2a and 2b) and summarized in (Table 6). The present Secondary Building Unit topology (SBU) is considered one of the most stable in the 1-D class exhibiting a drastic limited flexibility. As shown in Figure 4, the structure of the studied compound is self-assembled into alternating organic and inorganic layers parallel to the (bc) plane. The organic cations are in the voids around the face-sharing [PbI6] octahedra and form C–H· · ·I hydrogen interactions with iodine atoms I1 and I3 of different chains. In such packing, the organic moieties form an insulator barrier separating the semiconducting Pb2I6 chains. This periodic structure can be regarded as an organic–inorganic self-organized quantum wire structure as shown in Figure 3.

Table 4: Selected geometric parameters (Å, °) at 298 and 100 K

Bond	298 K	100 K	Bond	289 K	100K
Pb—I1 x 2	3.2013 (8)	3.1880 (6)	N2—C3	1.508 (14)	1.517 (13)
Pb—I3 x 2	3.2138 (8)	3.2011 (5)	N2—C2	1.514 (19)	1.523 (9)
Pb—I2 x 2	3.2733 (9)	3.2575 (5)	N2—C2^{iv}	1.508 (14)	1.523 (9)
N1—C1	1.451 (15)	1.468 (9)	N3—C1	1.494 (14)	1.474 (9)
N1—C3	1.42 (2)	1.432 (13)	N3—C2	1.414 (16)	1.436 (9)
N2—C5	1.47 (2)	1.479 (13)	N3—C4	1.469 (14)	1.469 (8)
I1—Pb—I1^{i}	180	180	N3—C4—N3^{iv}	110.3 (13)	113.1 (8)
I2—Pb— I2^{i}	180	180	N3—C2—N2	110.5 (10)	110.7 (6)
I3—Pb— I3^{i}	180	180	C1—N1—C1^{iv}	110.0 (14)	109.1 (8)
I1—Pb—I2	91.40 (2)	90.490 (14)	C2—N3—C4	110.5 (11)	107.6 (6)
I1—Pb—I3	91.27 (2)	88.620 (14)	C2—N3—C1	109.2 (10)	109.1 (6)
I2—Pb—I3	87.73 (2)	91.580 (14)	C2—N2— C2^{iv}	106.5 (8)	108.3 (8)
I1—Pb—I2^{i}	88.60 (2)	89.510 (14)	C3—N2—C2	106.5 (8)	107.5 (5)
I1—Pb—I3^{i}	88.73 (2)	91.379 (14)	C3—N1—C1	109.8 (9)	109.4 (5)
I3—Pb—I2^{i}	92.27 (2)	88.420 (14)	C3—N2—C2^{iv}	109.3 (12)	107.5 (5)
Pb—I1—Pb^{ii}	73.57 (2)	72.856 (15)	C4—N3—C1	108.5 (12)	108.8 (6)
Pb—I2—Pb^{iii}	71.70 (2)	71.062 (14)	C5—N2—C2	111.0 (13)	110.7 (5)
Pb—I3—Pb^{ii}	73.24 (2)	72.511 (14)	C5—N2—C2^{iv}	111.6 (9)	110.7 (5)
N1—C1—N3	109.6 (10)	111.4 (6)	C5—N2—C3	111.6 (9)	111.9 (8)
N1—C3—N2	111.2 (12)	110.6 (8)			

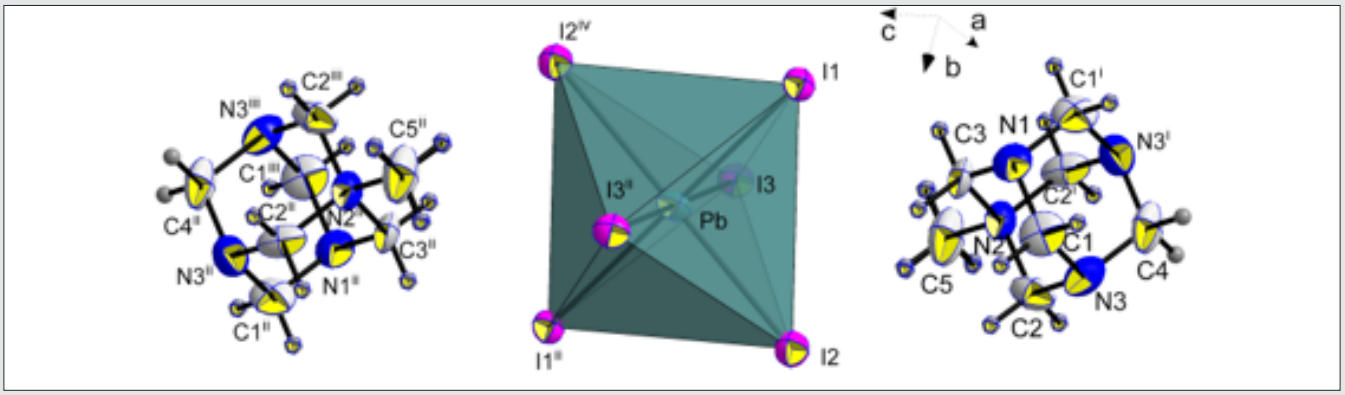

Figure 1: Structural units of the title compound at 298K, showing the atom-numbering scheme. Atomic displacement ellipsoids are drawn at 50 % probability level. [Symmetry codes: (i): x, 0.5-y, z; (ii):1-x, 0.5+y, 1-z; (iii):1-x, 1-y, 1-z; (iv):1-x, -0.5+y, 1-z].

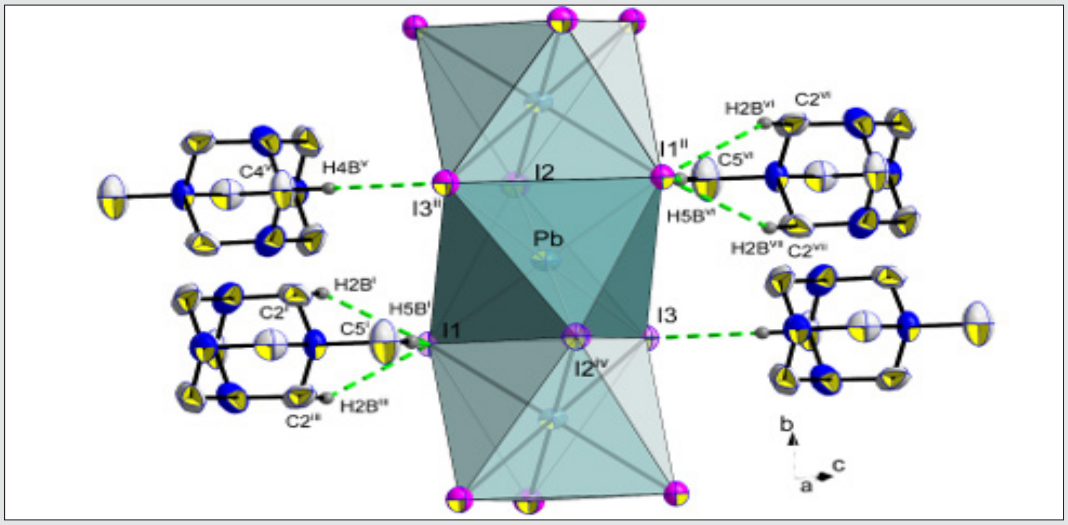

Figure 2a: A Linkage around [PbI6] octahedron. Hydrogen interactions are drawn as dashed green lines. [Symmetry codes: (i): x-1, y, z ; (ii):1-x, 0.5+y,1-z ; (iii):x-1, 0.5- y, z. (iv):1-x, -0.5+y, 1-z ; (v):1-x, 0.5+y, -z ; (vi):2-x, 0.5+y, 1-z ; (vii):2-x, 1-y, 1-z].

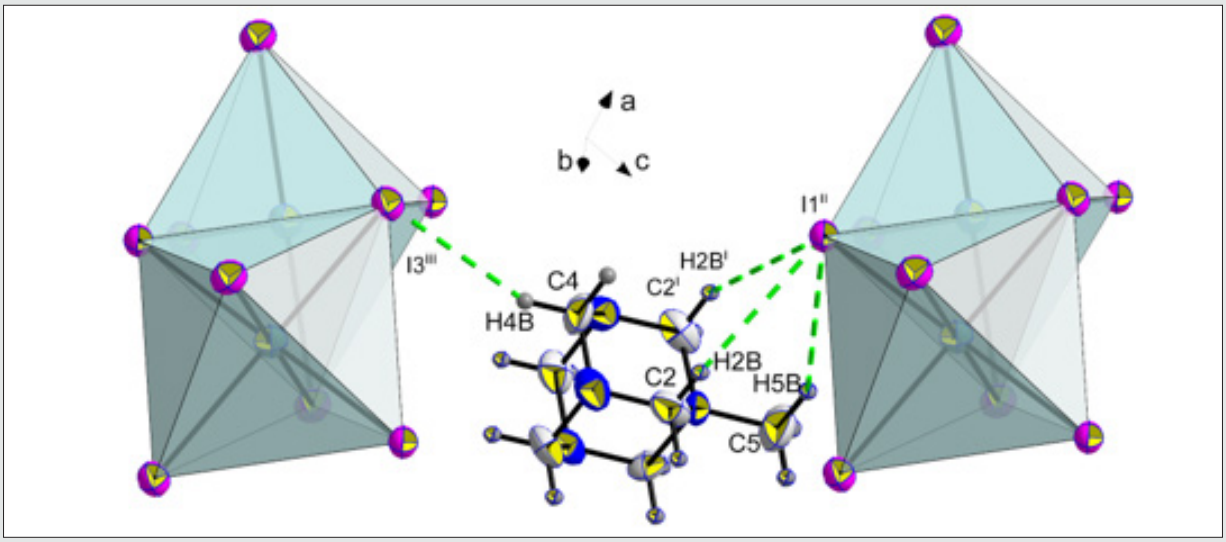

Figure 2b: Linkage around organic cation. Hydrogen interactions are drawn as dashed green lines. [Symmetry codes: (i): x, 0.5-y, z ; (ii):1+x, y, z ; (iii): x, y, z-1].

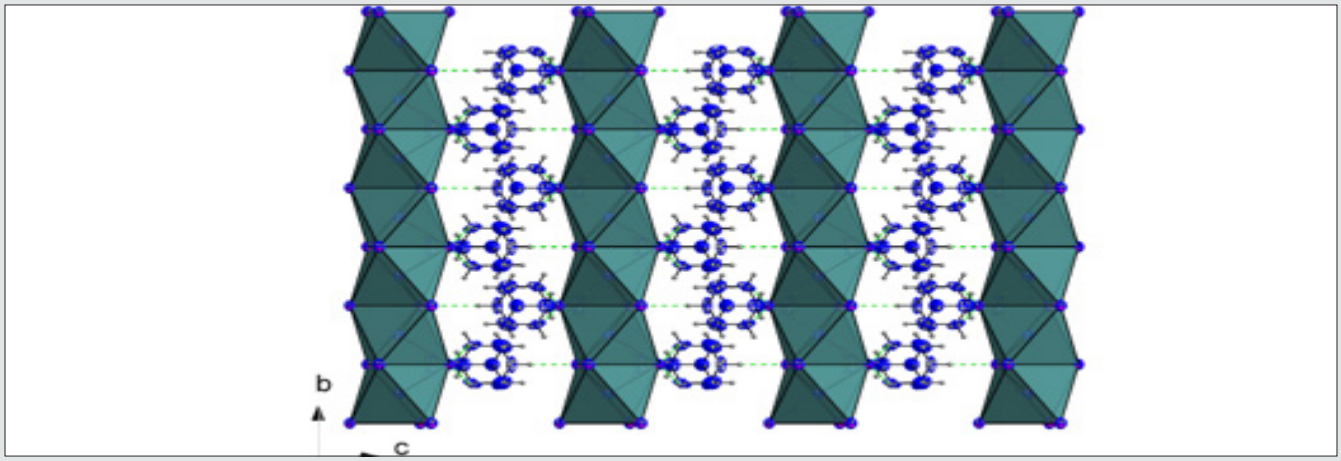

Figure 3: A packing diagram of (I), viewed along the axis showing the alternating organic and inorganic layers.

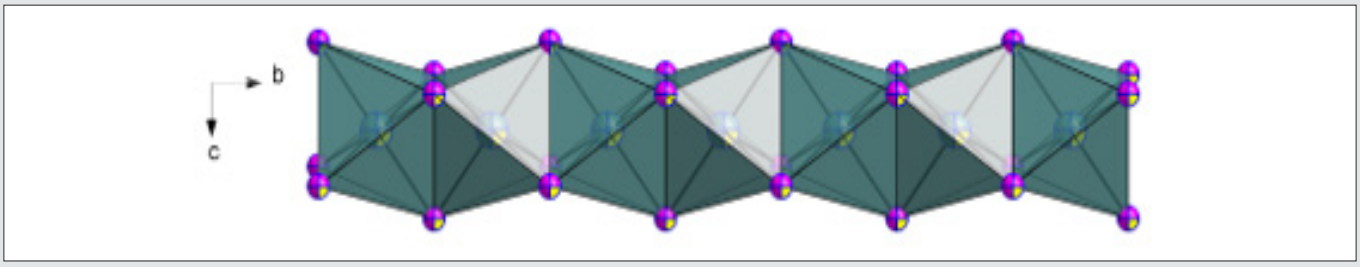

Figure 4: The [PbI6] ∞ chain of (I) running parallel to the a-axis direction and exhibiting a zigzag conformation.

Anionic neighboring

Every [PbI6] octahedra is sharing tow opposite triangular faces with tow homologous leading to a very stable 1-D linear topology. Only I1 and I3 and their symmetric are establishing interactions with the organic cations via weak C4—H4B···I3, C2—H2B···I1 and C5—H5B···I1 represented on Figure 2a (Table 5). Within the anionic network, the closest couple of lead cations are distant by dPb-Pb=3.834(2)Å which is nearly comparable to the theoretical value of DPb-Pb=1.16(dPb-I) of 3.75Å of the lead-based quantum wire structures using the averaged bond length dPb-I =3.229 Å. It' worth noting that every iodine is bi-coordinated.

Table 5: Hydrogen interaction geometry (dH…A<3.3 Å).

D—H···A	D—H (Å)		H···A(Å)		D···A(Å)		D—H···A (°)	
	298 K	100 K	298 K	100 K	298 K	100 K	298 K	100 K
C2—H2B···I1^{ii}	0.97	0.97	3.237	3.17	3.935(13)	4.051(7)	152.2	152.1
C2^{i}—H2B^{i}···I1^{ii}	0.97	0.97	3.237	3.17	4.121(11)	4.051(7)	152.2	152.1
C4—H4B···I3^{iii}	0.97	0.97	3.094	3.08	3.993(17)	3.993(10)	154.6	157.2
C5—H5B···I1^{ii}	0.96	0.96	3.286	3.16	4.155(2)	4.041(11)	151.6	153.5

Cationic neighboring

By limiting the considered inter-cationic hydrogen interaction (H…A) to 3.30Å summarized on (Table 5), the organic cations seem to be connected only to the iodine I1 and I3, vertices of the PbI6 octahedra. Thus, as shown on (Figure 2b), every organic cation is linked by four weak links C2-H2B...I1ii, C2i-H2Bi...I1ii, C5-H5B... I1ii and C4-H4B...I3iii ((i): x, 1/2-y, z; (ii) x+1, y, z; (iii) x, y, −1+z).

Similar structures

Searching to find comparable formulas to identify the role of every component in the studied structure, the "hexamethylenetetramine" (hmta) cation scheme was used in the "similarity" option of the WEBCSD interface. Only one lead metal organic-inorganic hybrid compound was identified. [22-30] The closest chemical composition found is: [2n($C_6H_{13}N_4$)

+, n(Pb2I62-)]17 (II). The title compound may be compared to selected previous work, yet it differs by the presence of the CH3 fragment generated by an alkylation reaction35 and coming from the DMSO used as solvent. The hydrogen atoms of the terminal CH3 group are engaged in weak hydrogen interactions ranging between 2.930 (2) Å and 3.286 (1) Å, strengthening the crystal cohesion.

Vibrational study

To gain information on interactions in the 2[(CH_3) $C_6N_4H_{12}$] +[Pb2I6]2- crystals, a vibrational study at room temperature was undertaken using infrared (IR) absorbance (Figure 5a) and Raman scattering (Figure 6). Based on the single crystal X-ray diffraction results and using CAChe program31, the calculated IR spectrum is shown in (Figure 5b) The vibrations of the studied compound can be attributed to internal vibrations of the organic cation, the translations of metal and iodide anions as well as lattice modes. The observed and calculated wavenumbers along with the assignment are given in (Table 6). The symbols used in the text have been explained in the footnote of this table. We have based our assignment mostly on the data available for the compounds containing amino hexamethylenetetramine (aHx) or lead halides 10 22 24 19 20. The mismatch between the calculated and observed frequencies is attributed to the approximations required in the computation algorithms. The main one relates to the assumption of isolated molecular units.

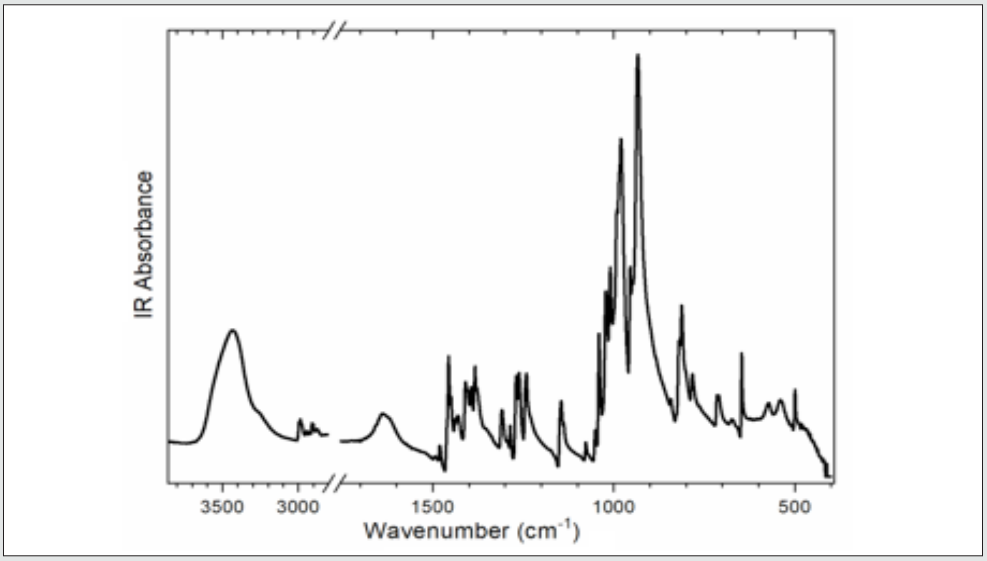

Figure 5a: Room temperature infrared spectrum of 2[(CH_3) $C_6N_4H_{12}$] +[Pb2I6]2-.

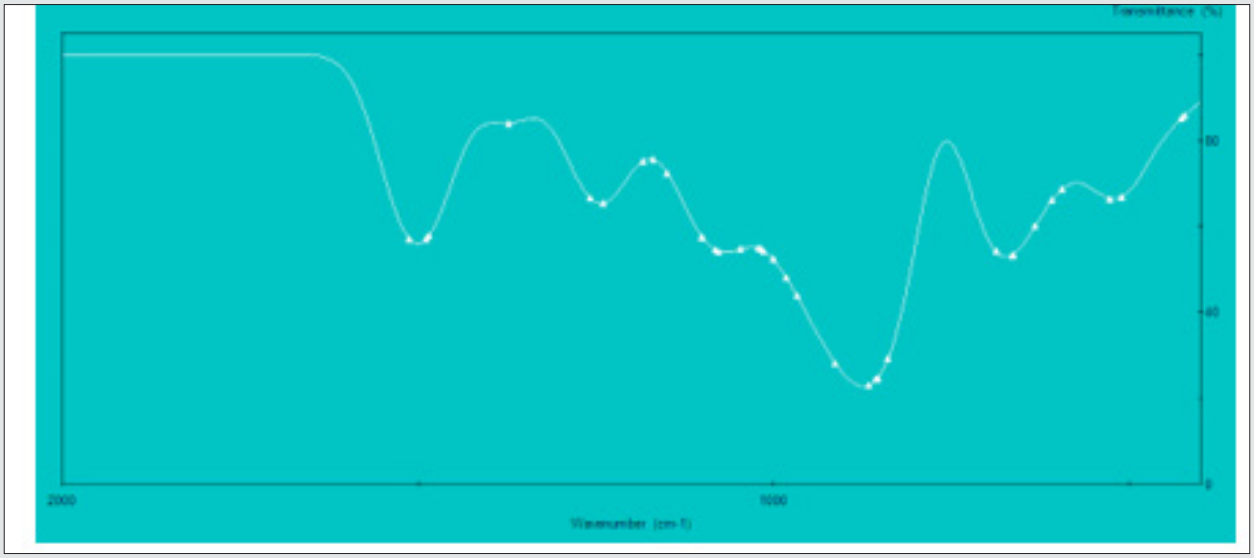

Figure 5b: Calculated infrared spectrum of 2[(CH_3) $C_6N_4H_{12}$] +[Pb2I6]2-.

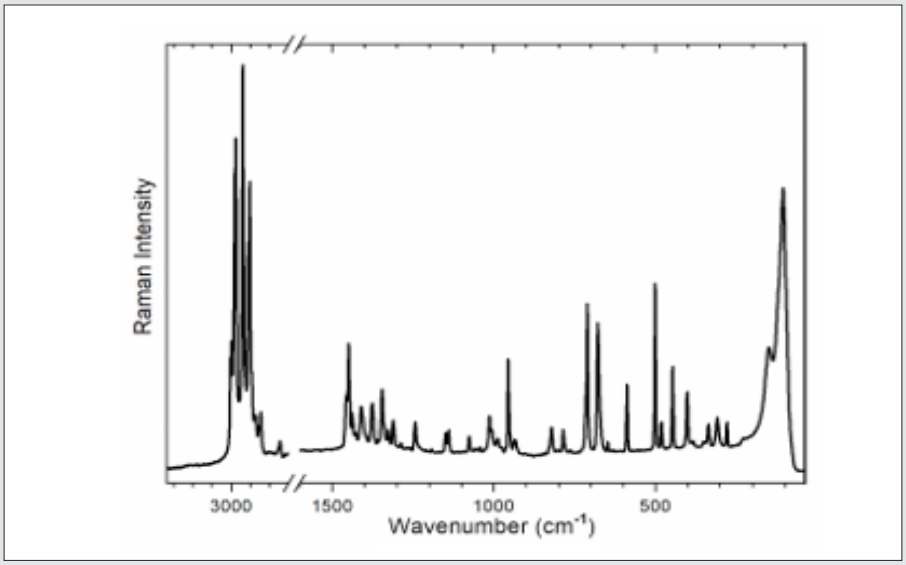

Figure 6: Raman spectrum of 2[(CH_3) $C_6N_4H_{12}$] +[Pb2I6]2-. recorded at room temperature.

Table 6: The wavenumbers (cm-1) of the observed Raman and infrared bands of 2[(CH_3) $C_6N_4H_{12}$] +[Pb2I6]2-.

Wave numbers (cm^{-1})			Assignment
FT-IR		FT-Raman	
observed	**calculated**	**observed**	
3427m			$\nu_{as}CH_3$
2994w 2988w 2979w		3005m 2997m 2981s 2975s	$\nu_{as}CH_2$ ν_sCH_3
2945w 2923w 2912w 2903w		2940vs 2912s 2904s	ν_sCH_2
2875w		2873vw 2846vw 2745vw	combination
1637m			$\delta_{as}CH_3$
1480w	1511 1487	1456m 1449m	δCH_2
1455m 1449m 1438w	1454	1438w 1427vw	δCH_2
1430w	1454		δ_sCH_3
1409m 1394m 1383m 1378m	1371	1411w 1375w 1345w 1325vw	ωCH_2
1309w	1371	1311w	τCH_2
1286w		1286vw	τCH_2
1269m 1261m 1241m	1257 1239	1243w	τCH_2
1145w	1183 1169 1149	1150vw 1139vw	$\nu_{as}CNC$
1077vw	1101 1099 1081 1077	1078w	νCN
1042vw 1051 vw	1046		ν_sCNC
1040m 1022m 1009m	1021 1014	1014w 1005vw	ρCH_2 ν_sCNC
991s 980s	1000 981	986vw	ρCH_2
955m 933vs	967 913	955m 935w	ρCH_2
819m 813m 783m	865 855 853 839	821w 785w	ρCH_2
715w 710w		711m 678m	νCN δCNC
647w	687 664 662 632 608	647w	δCNC
572w 539w 500w	594	588m	δCNC
540	527 511	501m 481w 446w	δCNC
	427 422	401w	δCNC

		336vw 309vw	T'aHx
		278vw	LaHx
		148m	LaHx
		105s	T'I T'Pb

Key: s-very strong, s-strong, m-medium, w-weak, vw-very weak, sh-shoulder; ν_s –symmetric stretching, ν_{as}: asymmetric stretching, δ: in-plane bending (scissoring), ρ: rocking, ω: wagging, τ: twisting (torsion), T'–translation, L–libration, aHx – aminohexamethylenetetramine.

The broad band centered at 3427 cm-1 in IR spectrum is attributed to the asymmetric stretching vibrations of NH3 group of the organic cation. Its symmetric stretching mode is placed at lower wavenumber in Raman spectrum; [31] however, it is superimposed by the CH_2 modes which have much stronger intensity here. The positions of the bands indicate that we should regard the hydrogen bonding formed by the HN_3 groups as weak according to T Steiner [32]. This agrees with the crystallographic data. The bands width is slightly broadened meaning that there are some ongoing anharmonic processes in the crystal as well as this may originate from the dynamical movements of the proton in the hydrogen bonding. However, temperature-dependent studies would be needed to confirm this fact.

Located within 3000-2900 cm^{-1}-1, the stretching vibrations of CH_2 groups are typical of the aHx cation. The asymmetric and symmetric stretching modes are active both in IR and Raman spectra confirming that some atoms of the organic cation are in the general positions. They are followed by multiple CH_2 deformation modes of different geometry found at the wavenumbers corresponding to ethylenediammonium molecules [33]. This proves that the hydrogen bonds do not affect the skeleton of the aHx cations. The shapes of the bands corresponding to the CH_2 and other modes of the molecule's core also demonstrate that they are well ordered at room temperature since disordering leads to their broadening [34]. The lattice modes are observed roughly below 400 cm^{-1}. They originate mostly from the translations and vibrations of the organic cation as well as the translations of lead and iodide anions. The most intense band at 148 cm-1 in Raman spectrum has been ascribed to the vibration of the organic cage-like molecule while the band at 105 cm-1 have been assigned to the translations of iodide and lead, corresponding to the stretching modes of the Pb–I bonds if the analysis is based overall PbI6 octahedron. This agrees with other lead-iodide-based systems

Photoluminescence Property

2[(CH_3) $C_6N_4H_{12}$] +[Pb_2I_6]2- photoluminescence spectrum (Figure 7) exhibits two distinct emission bands centered at 2.43 eV and 3.05 eV, like those reported for other organic–inorganic perovskite 52526. The photoluminescence at 3.05 eV can be related to an excitonic transition [35-38]. The strong narrow peak at 2.43 eV is assigned to the charge-transfer transition between the two-dimensional inorganic layers sandwiched between the organic layers 27 20. The GAP energy was determined by the extrapolation of the linear part of the first peak, the value obtained is equal to 2.08 eV.

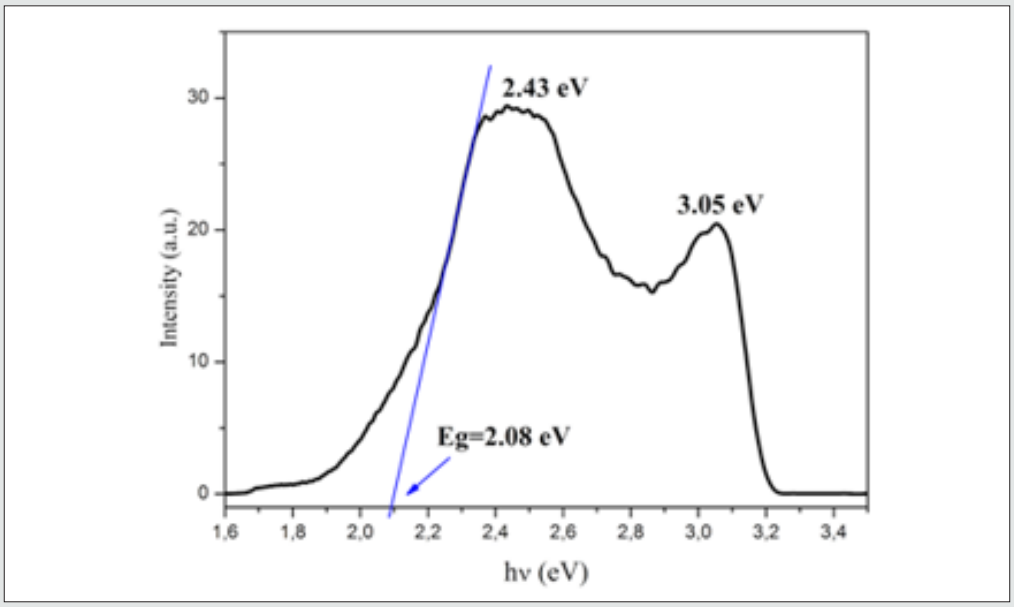

Figure 7: Photoluminescence (PL) spectrum of 2[(CH_3) $C_6N_4H_{12}$] +[Pb2I6]2-.

The HOMO-LUMO gap

The studied crystalline materials exhibit an interesting, calculated band gap around (-1.102) - (-1.118) = 0.016 eV corresponding to the electronic transition from the Highest Occupied Molecular Orbital (HOMO) to the Lowest Unoccupied Molecular Orbital (LUMO). Based on the structural investigations results, the computation and the graphical output were carried out using CAChe program [31]. Represented on (Figure 8), both HOMO and LUMO are localized on the organic and inorganic moieties. The low HOMO–LUMO energy gap of 0.016 eV indicates that the material can have interesting conduction properties to be verified by further experiments.

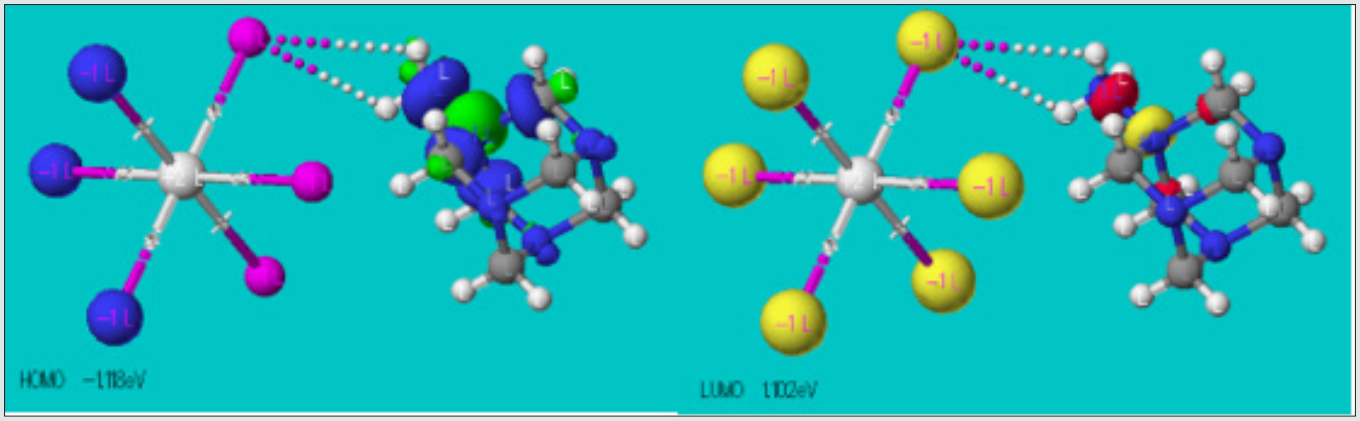

Figure 8: The spatial plot of HOMO and LUMO orbitals in the structure of 2[(CH_3) $C_6N_4H_{12}$] +[Pb2I6]2-.

Crystal morphology

Crystal morphology is a key element in many industrial processes and has an enormous impact in the materials processing stages. Thus, rationalization of the relationships between crystal morphology and the arrangement of atoms in the bulk crystal lattice is of great interest in many areas of science. In this way, we wanted to provide a comprehensive understanding of the crystal structure-morphology relationships in this material. To predict which crystal faces are most likely to appear in its morphology, the BFDH model29,30 was used, based on the symmetry of the crystal lattice to generate a significant list of possible growing faces. (Figure 9) represents the calculated crystal morphology using Mercury (CSD 3.0.1)36 showing that (001) and (00-1) faces are the most important growth directions. This can be interpreted accordingly to the Fig. 3 where the [001] crystal packing direction is clearly shown.

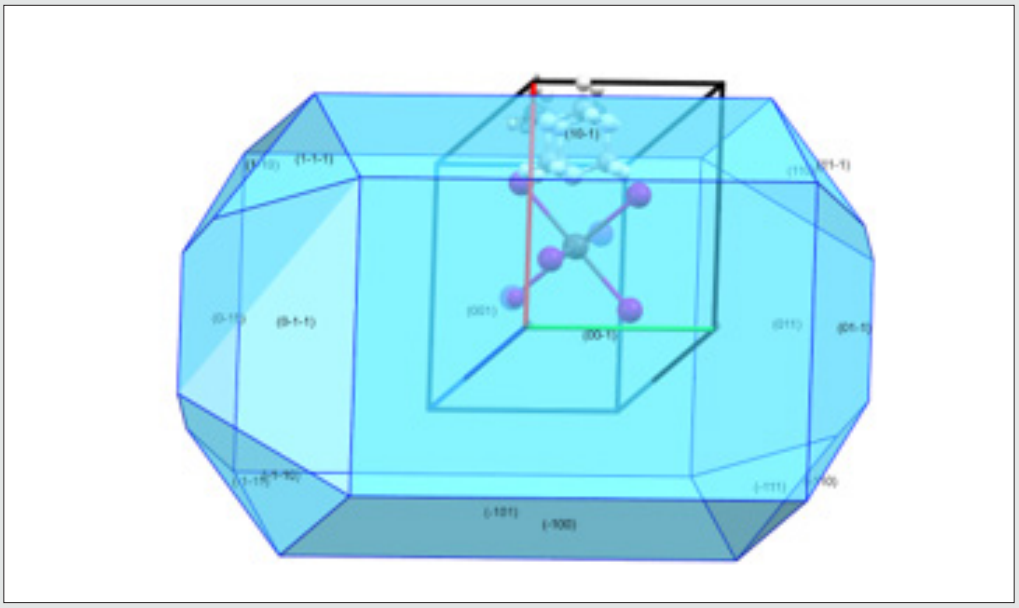

Figure 9: Predicted crystal morphology of 2[(CH_3) $C_6N_4H_{12}$] +[Pb2I6]2-from BFDH rules.

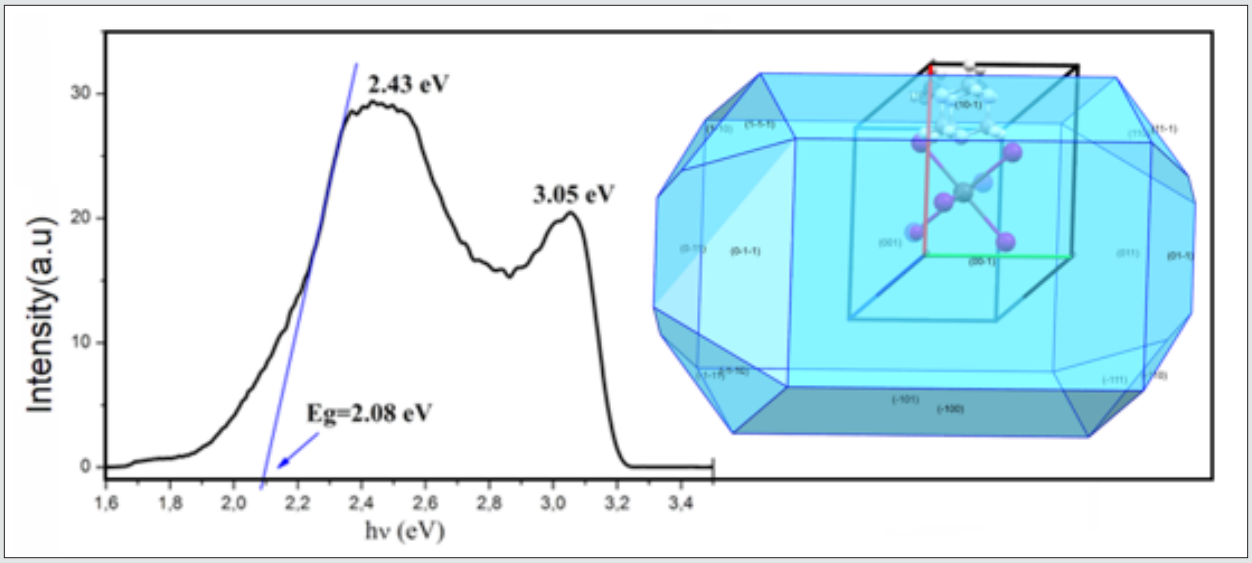

Graphical Abstract

Temperature effects on the crystal structure

Comparing the crystal structure at ambient and low temperature, in addition to the atomic Deby-Waller factors, significant changes in the cell parameters, unit cell volume, bond lengths and angles are noted. Indeed, by increasing temperature from 100K to 298 K, the cell parameters are expanding with an obvious increasing of the atomic displacement factors, the Pb-I bond length are getting longer and, surprisingly, those of the organic cation are getting shorter as resumed on (Table 4). On the other hand, no global tendency variation related to the hydrogen interaction and the bond length angles can be noted.

Conclusion

In summary, we have reported in this work, the synthesis, the structural investigation, the vibrational and optical properties of a new organic–inorganic crystal $2[(CH_3)\ C_6N_4H_{12}]$ +[Pb2I6]2-. The compound has been synthesized and its structure elucidated by single crystal X-ray diffraction at low and room temperature. The structure exhibits inorganic chains of face-sharing octahedra alternating the organic cations connected by weak C-H···I hydrogen interactions leading to a 3D network and ensuring the cohesion of the crystal structure. There are no major structural differences between the structures at low and room temperature other than the cell dimension and the atomic displacement factors expansion, lengthening of the inorganic bond's length and the shortening of the organic ones respectively at low and room temperature. Moreover, the vibrational study has been carried out by means of FT-IR and Raman spectroscopy, which confirms the rather weak hydrogen bonding in the material as estimated by X-ray diffraction. The absence of band broadening indicates that the molecules are well ordered at room temperature. The semi empirical PM3 treatment allows calculating the IR frequencies. The crystal shape morphology was simulated using the Bravais-Friedel and Donnay-Harker model. The band gap energy indicates that the compound behaves as a conductor material. A strong photoluminescence emission at room temperature is noted, which can be ascribed to many factors in particular the recombination of self-trapped exciton in the (PbI6) ∞ quantum wires and the charge-transfer phenomena from the inorganic chains to the organic molecules. The difference between the values of theoretical and experimental gap energy can be attributed to impurities in the sample. More experiments and theoretical studies could be useful to elucidate the electronic structure and to understand electronic interactions between inorganic and organic molecules in this novel compound.

References

1. Billing, DG, Lemmerer A (2006) catena-Poly [bis(tert-butylammonium) [plumbate (II)-tri-μ-iodo] iodide dihydrate]. Acta Crystallographica Section C: Crystal Structure Communications 62(6): 264-266.
2. Elleuch S, Boughzala H, Driss A, Abid YA (2007) one-dimensional organic–inorganic hybrid compound [(CH3)2CNHCH2CH2CH3] [PbI3]. Acta Crystallographica Section E: Structure Reports Online 63(2): 306-308.
3. Shahverdizadeh GH, Soudi AA, Morsali A, Retailleau P (2008) Four mixed-ligands lead (II) complexes based on 8-hydroxyquinolin (8-HQuin), [Pb(8-Quin)X]; X=4-pyridinecarboxylate, acetate, thiocyanate and nitrate; structural and thermal studies. Inorganica Chimica Acta 361(7): 1875-1884.
4. Kessentini A, Belhouchet M, Suñol J, Abid Y, Mhiri T, et al. (2013) Synthesis, crystal structure, vibrational spectra, optical properties and theoretical investigation of bis (2-aminobenzimidazolium) tetraiodocadmate. Journal of Molecular Structure 1039: 207-213.
5. Pradeesh K, Agarwal M, Rao KK, Prakash GV (2010) Synthesis, crystal structure and optical properties of quasi-one-dimensional lead (II) iodide: C14H18N2Pb2I6. Solid State Sciences 12(1): 95-98.
6. Abid H, Samet A, Dammak T, Mlayah A, Hlil E, et al. (2011) Electronic structure calculations and optical properties of a new organic-inorganic luminescent perovskite:(C9H19NH3)2PbI2Br2. Journal of Luminescence 131(8): 1753-1757.

7. Zheng YY, Wu G, Chen HZ, Wang M (2007) Bis [N-(1-naphthyl) ethylenediammonium] hexaiodoplumbate (II). Acta Crystallographica Section E: Structure Reports Online 63 (2): 504-506.
8. Yang JH, Zheng SL, Yu XL, Chen XM (2004) Syntheses, structures, and photoluminescent properties of three silver (I) cluster-based coordination polymers with heteroaryl dicarboxylate. Crystal growth & design 4 (4): 831-836.
9. Li JP, Li LH, Wu LM, Chen L (2009) Synthesis, properties, and theoretical studies of new stepwise layered iodoplumbate: [Ni(opd)2(acn)2] n[Pb4I10]n. Inorganic chemistry 48(4): 1260-1262.
10. Nandi P, Giri C, Joseph B, Rath S, Manju U, et al. (2016) CH3NH3PbI3, a potential solar cell candidate: Structural and spectroscopic investigations. The Journal of Physical Chemistry A 120(49): 9732-9739.
11. Mitzi DB (2001) Templating and structural engineering in organic–inorganic perovskites. Journal of the Chemical Society, Dalton Transactions 1(1): 1-12.
12. Mitzi DB, Liang K, Wang S (1998) Synthesis and characterization of [NH3C(I)NH3]2ASnI5 with A= iodoformamidinium or formamidinium: The chemistry of cyanamide and tin (ii) iodide in concentrated aqueous hydriodic acid solutions. Inorganic Chemistry 37(2): 321-327.
13. Xcalibur C (2008) System CrysAlis CCD and CrysAlis RED. Oxford Diffraction Ltd, Abingdon, England.
14. Sheldrick GM (2008) A short history of SHELX. Acta Crystallographica Section A: Foundations of Crystallography 64(1): 112-122.
15. Sheldrick GM (2015) SHELXT–Integrated space-group and crystal-structure determination. Acta Crystallographica Section A: Foundations and Advances 71(1): 3-8.
16. Hübschle CB, Sheldrick GM, Dittrich B (2011) ShelXle: A Qt graphical user interface for SHELXL. Journal of applied crystallography 44(6): 1281-1284.
17. Miyamae H, Nishikawa H, Hagimoto K, Hihara G, Nagata M, et al. (1988) Crystal Structures of Compounds Obtained from Lead (II) Iodide-Hexamethylenetetramine System, [C6H13N4]2[Pb3I8 (C6H12N4)2] and [C6H13N4] [PbI3M3]. Chemistry Letters 17(11): 1907-1910.
18. Preda N, Mihut L, Baibarac M, Baltog I (2007) Raman and photoluminescence studies on low-dimensional PbI2 particles embedded in polymer matrix. Journal of Optoelectronics and Advanced Materials 9 (5): 1358-1361.
19. Bertie JE, Solinas MJ (1974) Infrared and Raman spectra and the vibrational assignment of hexamethylenetetramine-h_{12} and -d_{12}. Chem Phys 61(5): 1666-1667.
20. Perez-Osorio M, Milot R, Filip MR, Patel JB, Herz LM, et al. (2015) Vibrational Properties of the Organic–Inorganic Halide Perovskite $CH_3NH_3PbI_3$ from Theory and Experiment: Factor Group Analysis, First-Principles Calculations, and Low-Temperature Infrared Spectra. J. Phys. Chem. C 119(46): 25703-25718.
21. Preda N, Mihut L, Baibarac M, Baltog I, Lefrant S, et al. (2006) A distinctive signature in the Raman and photoluminescence spectra of intercalated PbI_2. Journal of Physics: Condensed Matter 18(39): 8899.
22. Amerling E, Baniya S, Lafalce E, Zhang C, Vardeny Z V, et al. (2017) Electroabsorption Spectroscopy Studies of $(C_4H_9NH_3)2PbI_4$ Organic-Inorganic Hybrid Perovskite Multiple Quantum Wells. The journal of physical chemistry letters 8(18): 4557-4564.
23. Niemann RG, Kontos AG, Palles D, Kamitsos EI, Kaltzoglou A, et al. (2016) Halogen effects on ordering and bonding of CH_3NH_3 in $CH_3NH_3PbX_3$ (X= Cl, Br, I) hybrid perovskites: a vibrational spectroscopic study. The Journal of Physical Chemistry C 120(5): 2509-2519.
24. Refat MS, Sharshar T (2012) Infrared, Raman, 1H NMR, thermal and positron annihilation lifetime studies of Pb (II), Sn (II), Sb (III), Bi (III)-barbital complexes. Journal of Molecular Structure 1016: 140-146.
25. Green MA, Jiang Y, Soufiani AM, Ho-Baillie A (2015) Optical properties of photovoltaic organic–inorganic lead halide perovskites. The journal of physical chemistry letters 6(23): 4774-4785.
26. Shkir M, Yahia I, AlFaify S, Abutalib M, Muhammad S, et al. (2016) Facile synthesis of lead iodide nanostructures by microwave irradiation technique and their structural, morphological, photoluminescence and dielectric studies. Journal of Molecular Structure 1110: 83-90.
27. Baltog I, Baibarac M, Lefrant S (2008) Quantum well effect in bulk PbI2 crystals revealed by the anisotropy of photoluminescence and Raman spectra. Journal of Physics: Condensed Matter 21(2): 025507.
28. Brandenburg K, Putz K (2008) Diamond Ver. 3.1, Crystal Impact GbR. Bonn, Germany.
29. Bravais A (1866) Études cristallographiques. Gauthier-Villars
30. Donnay JDH, Harker D (1937) Springer Handbook of crystal growth. American Mineralogist pp. 446-467.
31. CAChe: work system Pro Version 7.5.0.85, Fujitsu Limited. 2000-2006 Oxford Molecular, USA.
32. Steiner T (2002) The Hydrogen Bond in the Solid State. Willey Online Library 41(1): 48-76.
33. Trzebiatowska M, Zarychta B, Pikul A, Mączka M, Peksa P, et al. (2017) Polar metal–formate frameworks templated with 1,2-diaminoethane–water assemblies showing ferromagnetic and ferroelectric properties. Phys Chem Chem Phys 19(25): 16749-16757.
34. Trzebiatowska M, Ptak M (2019) the mechanism of phase transitions in azide perovskites probed by vibrational spectroscopy. Spectrochim Acta A 214: 184-191.
35. Kaihua J, Shuhong B (2018) Coordination Compounds of Hexamethylenetetramine with Metal Salts: A Review. Johnson Matthey Technology Review 62(1): 4-31.
36. Macrae CF, Bruno IJ, Chisholm JA, Edgington PR, McCabe P, et al. (2008) Mercury CSD 2.0 -new features for the visualisation and investigation of crystal structures. J Appl Crystallogr 41: 466-470.
37. Groom CR, Bruno IJ, Lightfoot MP, Ward SC (2016) The Cambridge Crystallographic Data Centre. Acta Cryst B72: 171-179.

DOI: 10.32474/AOICS.2021.05.000216